NMR structure of the bovine prion protein

Francisco López García, Ralph Zahn, Roland Riek, and Kurt Wüthrich*

Institut für Molekularbiologie und Biophysik, Eidgenössische Technische Hochschule, Hönggerberg, CH-8093 Zürich, Switzerland

Contributed by Kurt Wüthrich, May 15, 2000

The NMR structures of the recombinant 217-residue polypeptide chain of the mature bovine prion protein, bPrP(23–230), and a C-terminal fragment, bPrP(121–230), include a globular domain extending from residue 125 to residue 227, a short flexible chain end of residues 228–230, and an N-terminal flexibly disordered ''tail'' comprising 108 residues for the intact protein and 4 residues for bPrP(121–230), respectively. The globular domain contains three α-helices comprising the residues 144–154, 173–194, and 200–226, and a short antiparallel β-sheet comprising the residues 128–131 and 161–164. The best-defined parts of the globular domain are the central portions of the helices 2 and 3, which are linked by the only disulfide bond in bPrP. Significantly increased disorder and mobility is observed for helix 1, the loop 166–172 leading from the β-strand 2 to helix 2, the end of helix 2 and the following loop, and the last turn of helix 3. Although there are characteristic local differences relative to the conformations of the murine and Syrian hamster prion proteins, the bPrP structure is essentially identical to that of the human prion protein. On the other hand, there are differences between bovine and human PrP in the surface distribution of electrostatic charges, which then appears to be the principal structural feature of the ''healthy'' PrP form that might affect the stringency of the species barrier for transmission of prion diseases between humans and cattle.

Bovine spongiform encephalopathy (BSE) or ''mad cow disease'' has in recent years been outstandingly visible among the transmissible spongiform encephalopathies (TSEs) or ''prion diseases.'' An intense discussion is focused on the likelihood that BSE could be transmitted to humans through the food chain, causing ''new variant Creutzfeldt–Jakob disease'' (nvCJD) (1–8). Although laboratory experiments provided contradictory evidence with regard to a stringent species barrier for infectious transmission of BSE to primates via the oral route (9, 10), there are strong indications that this species barrier might be crossed in real life, with humans ingesting beef in their daily diet.

On the molecular level the onset of TSEs has been related to a change in the three-dimensional structure of the host-encoded prion protein, PrP, with conversion of the ubiquitous ''cellular form'' of PrP, PrP^{C}, into a disease-related ''scrapie form,'' PrP^{Sc}, which is found as highly aggregated deposits in the brain of individuals with advanced stages of TSEs. The ''protein-only'' hypothesis (11–14) actually proposes that PrP^{Sc} is the causative agent of prion diseases. Studies of three-dimensional prion protein structures have therefore attracted keen interest, and nuclear magnetic resonance (NMR) solution structures have been described of the monomeric, cellular forms of the prion proteins from the mouse, mPrP (15–18), the Syrian hamster, shPrP (19–21), and humans, hPrP (22). These three proteins have closely similar global folds characterized by the presence of a flexible, ''unstructured'' 100-residue N-terminal ''tail'' attached to a globular domain of nearly identical size, but they also show localized structure variability that might be related with the species barrier for infectious transmission of TSEs. We have now extended the structural investigations to the intact recombinant 217-residue bovine prion protein, bPrP(23–230) (see ref. 23 for the numeration used) and its C-terminal fragment bPrP(121–230). The bPrP structure is compared with the other available mammalian PrP structures (15–22), and the observed structure variations are related to those in a group of single-amino acid variants of hPrP(121–230) (24).

Materials and Methods

Recombinant bPrP polypeptides with and without isotope labeling (for details see *Results*) were prepared by the procedures described previously for hPrP polypeptides (22, 25). For the NMR structure determinations of bPrP(23–230) and bPrP(121–230), the procedures used were identical to those in the following paper (24).

For the hydrogen–deuterium exchange studies, H_2O solutions of ^{15}N-labeled bPrP(23–230) or bPrP(121–230) were lyophilized, the protein was redissolved in $^{2}H_2O$ (D_2O), and a series of 20 two-dimensional [^{15}N,^{1}H]-correlation spectroscopy spectra were recorded within 1,790 min, with a time domain data size of 128 × 1024 complex points, $t_{1,max}(^{15}N) = 54$ ms and $t_{2,max}(^{1}H) = 108$ ms. Protection factors were obtained by fitting the data to single-exponential decays and accounting for the sequence effects on the random coil exchange rates (26).

Steady-state $^{15}N\{^{1}H\}$-nuclear Overhauser enhancements (NOEs) and ^{15}N spin-relaxation times were measured following ref. 27. For the NOE measurements we used a recovery delay of 3 s and a proton saturation period of 3 s. For the measurement of longitudinal ^{15}N-spin relaxation times, $T_1(^{15}N)$, a series of 10 spectra was recorded with relaxation delays between 15 and 1,500 ms. Transverse ^{15}N relaxation times, $T_2(^{15}N)$, were obtained from a series of 10 spectra with relaxation delays between 10 and 280 ms. For all relaxation measurements we used $t_{1,max}(^{15}N) = 54$ ms and $t_{2,max}(^{1}H) = 108$ ms, and a time domain data size of 128 × 1024 complex points. The data were analyzed with the program DASHA (28).

Results

For the present study the polypeptides bPrP(23–230) and bPrP(121–230) were prepared without isotope labeling, uniformly ^{15}N-labeled, and uniformly ^{13}C,^{15}N-labeled, and we also used a 10% ^{13}C-labeled sample of bPrP(121–230). For the structure determination we used 1 mM protein solutions either in 90% H_2O/10% D_2O or in 99.9% D_2O, with addition of 10 mM sodium acetate and 0.05% sodium azide at a pH meter reading of 4.5 and 20°C.

Abbreviations: NOE, nuclear Overhauser enhancement; $^{15}N\{^{1}H\}$-NOE, heteronuclear Overhauser enhancement of ^{15}N after saturation of ^{1}H; PrP, prion protein; PrP^{C}, cellular form of PrP; PrP^{Sc}, scrapie form of PrP; bPrP(23–230), complete polypeptide chain of the mature bovine PrP, which contains 217 amino acid residues (see ref. 23 for the numeration used); bPrP(121–230), fragment of bovine PrP comprising residues 121–230; hPrP(23–230), complete polypeptide chain of the mature human PrP; hPrP(121–230), fragment of human PrP comprising residues 121–230; mPrP(121–231), fragment of mouse PrP comprising residues 121–231; shPrP(90–231) fragment of Syrian hamster PrP comprising residues 90–231; TSE, transmissible spongiform encephalopathy.

Data deposition: Atomic coordinates for a bundle of 20 conformers and for the best conformer of the fragment of residues 124–227 in bPrP(121–230) and bPrP(23–230) have been deposited in the Protein Data Bank, www.rcsb.org (PDB ID codes 1DWY, 1DWZ, 1DX0, and 1DX1).

*To whom reprint requests should be addressed. Fax: 41-1-633-1151.

The publication costs of this article were defrayed in part by page charge payment. This article must therefore be hereby marked "*advertisement*" in accordance with 18 U.S.C. §1734 solely to indicate this fact.

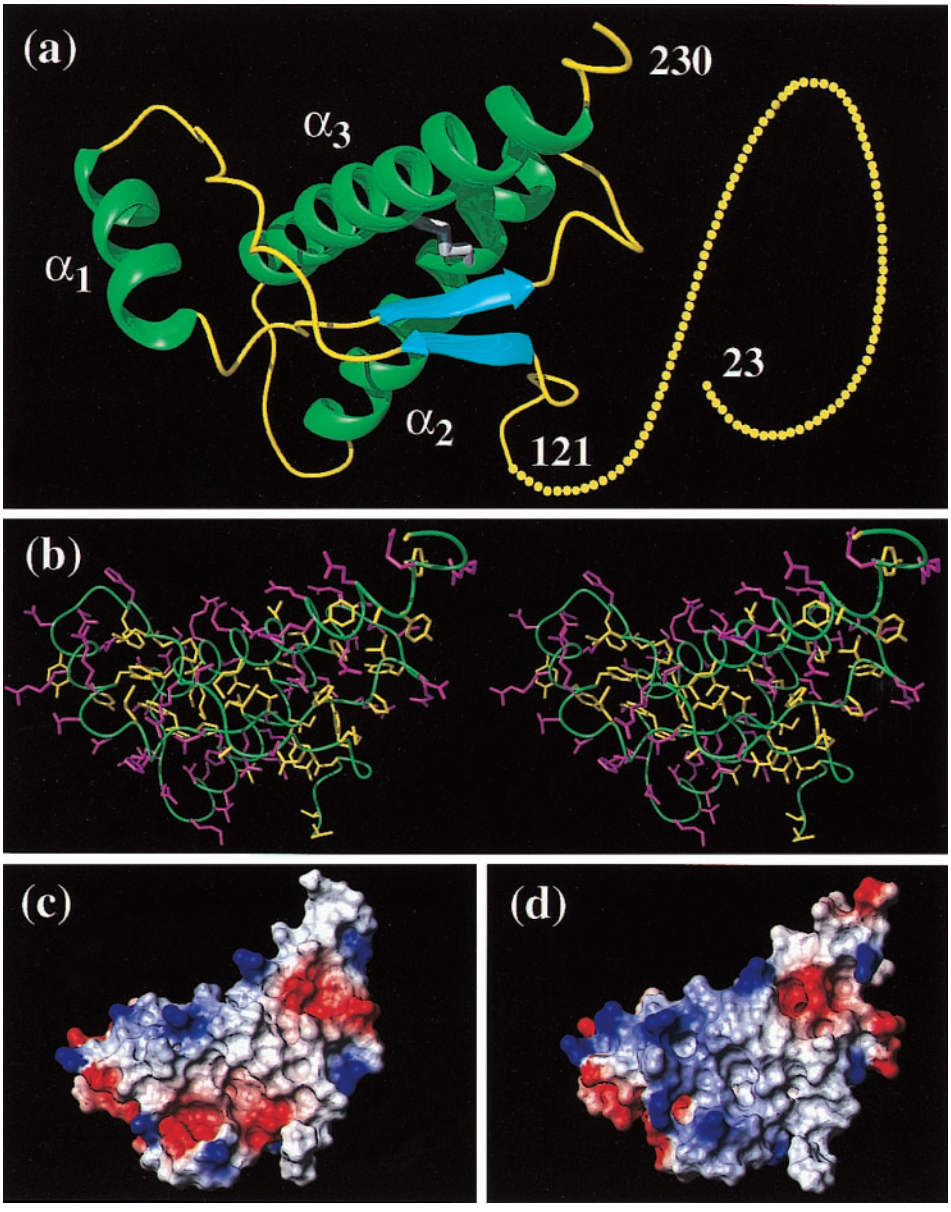

Fig. 1. (*a*) Cartoon of the three-dimensional structure of the intact bPrP(23–230). Helices are green, β-strands are cyan, segments with nonregular secondary structure within the C-terminal domain are yellow, and the flexibly disordered ''tail'' of residues 23–121 is represented by 108 yellow dots, each of which represents a residue of the tail (the numeration for hPrP is used, and the insertions and deletions are placed according to the alignment in ref. 23). (*b*) Stereo-view of an all-heavy atom presentation of the globular domain in bPrP(23–230), with residues 121–230, in the same orientation as in *a*. The backbone is shown as a green spline function through the C^{α} positions, hydrophobic side chains are yellow, and polar and charged side chains are violet. (*c* and *d*) Surface views of the globular domains of bPrP and hPrP, respectively. The orientation of the molecule is slightly changed relative to *a*, so that the residue 186 is approximately in the center. The electrostatic surface potential is indicated in red (negative charge), white (neutral), and blue (positive charge). The figures were prepared with the program MOLMOL (42).

The NMR structure of the recombinant bPrP(23–230) (Fig. 1*a*) contains a globular domain that extends approximately from residue 122 to residue 227, where the residues 128–131 form the β-strand 1, 144–154 the α-helix 1 (which has 3_{10}-type structure from residue 153 onward), 161–164 the β-strand 2, 173–194 the α-helix 2, and 200–226 the α-helix 3. At both ends of the globular domain there are flexibly disordered polypeptide segments, as evidenced by near-random coil ^{1}H chemical shifts (29) and negative values of the steady-state ^{15}N{^{1}H}-NOEs (Fig. 2). The N-terminal tail comprising residues 23–121 (because of insertions relative to hPrP this segment includes 108 residues; see ref. 23 for the numeration used) shows exclusively negative NOEs, and because of signal overlap only one set of values was obtained for all six octapeptide segments (23), as indicated by the box in Fig. 2. The positive NOEs for residues 122–227 are typical for a globular protein of this size (see also below), whereas increased flexibility is again indicated for the C-terminal tripeptide segment (Fig. 2).

Resonance Assignments and Structure Determination. For the globular domain of residues 121–230 in bPrP(23–230) and bPrP(121–230), nearly complete assignments were obtained for the polypeptide backbone and the aliphatic CH_n groups of the amino acid side chains, the exceptions in both proteins being the backbone amide protons of Asp-167, Ser-170, Asn-171, and Phe-175, and H^{α} and H^{β} of Phe-175. At least one

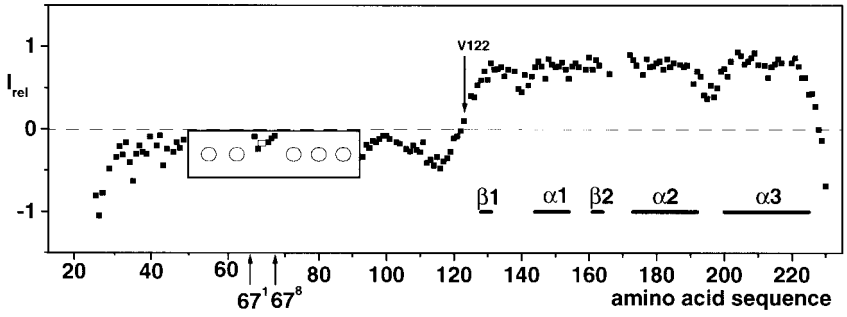

Fig. 2. Steady-state $^{15}N\{^1H\}$-NOEs of the backbone amide groups measured in a 1 mM solution of bPrP(23–230) in 90% H_2O/10% D_2O containing 10 mM sodium acetate at pH 4.5 and 20°C. In the box enclosing positions 51–91 the pattern of NOE values is indicated for the octapeptide repeat that is inserted between the positions 67 and 68 (hPrP numbering, see ref. 23), where the open rectangle indicates that only one value was measured for two Gly residues. The circles indicate that identical patterns prevail for the other five repeats (see text). The regular secondary structures in the C-terminal globular domain are indicated at the bottom, and the first residue with a positive NOE value, Val-122, is identified.

heteronuclear sequential scalar connectivity (30) or one sequential NOE (29) has been observed for each pair of neighboring residues, except for 166–167, 167–168, 169–170, 170–171, and 174–175. The Xaa-Pro peptide bonds with the prolines 137, 158, and 165 are in the *trans* conformation, as evidenced by the observation of strong $d_{\alpha\delta}$ NOEs (29). Assignments were obtained for all 11 Tyr rings and the 3 Phe and 4 His rings, with the sole exceptions of εCH of His-155 and His-187, and ζCH of Phe-198. The amide groups of the 7 Asn and 8 Gln residues, the ε-proton resonances of the 8 Arg residues, and the hydroxyl proton of Thr-183 were assigned by intraresidual NOEs (29). Stereospecific assignments for the methyl groups of the 13 valyl and leucyl isopropyl moieties in bPrP(121–230) were obtained by biosynthetically directed fractional ^{13}C labeling (31, 32) and then transferred to bPrP(23–230).

In the N-terminal tail of bPrP(23–230), nearly complete sequence-specific assignments were obtained for the residues 23–50 and 92–120. For the six "octapeptide repeats" ⟨Pro-His/Gln-Gly-Gly-Gly-⟩Gly⟨Trp-Gly-Gln⟩ from positions 51 to 91 (23), sequence-specific assignments were obtained only for the tripeptide segment Pro-Gln-Gly at residues 51–53 and the dipeptide Gly-Gln at residues 90–91, because chemical shift degeneracy prevented further assignments of individual residues (see Fig. 2).

For both proteins, bPrP(23–230) and bPrP(121–230), a structure determination was performed for the polypeptide segment of residues 121–230, using the program DYANA (33). The input for the final structure calculation of the segment 121–230 contained 1,576 and 1,797 NOE upper distance limits for bPrP(23–230) and bPrP(121–230), and there were 469 and 483 dihedral angle constraints, respectively (Table 1). The same protocol was used for the structure calculation as in the following paper (24), and the results are given in Table 1.

The Globular Domain. The domain in bPrP(23–230) is very similar to that in bPrP(121–230) (Fig. 3*a*), with an rms deviation value of 0.64 Å between the backbone heavy atoms of residues 125–227 in the mean structures of the two proteins. The near-identity includes the regular secondary structure elements, the core amino acid side chains [Fig. 1*b*; for clarity only the all-atom presentation of the domain in bPrP(23–230) is shown], the hydrogen bonding network with similar long-range connections as in mPrP(121–231) (18), and the variable precision of the structure determination along the sequence (Fig. 3*a*).

The nature of the structural disorder manifested in increased mean atomic displacements for some segments of the polypeptide chain (Fig. 3*a*) has been probed by amide proton exchange experiments (Fig. 4) and spin-relaxation measurements (Fig. 5). The amide proton protection factors of bPrP(23–230) and bPrP(121–230) differ only for the residues 134, 221, and 222 (Fig. 4). In the regular secondary structures only the residues 188–194 in helix 2 and residues 221–226 in helix 3 (Fig. 4) are not measurably protected against exchange, which coincides with the reduced precision of the structure determination for these residues (Fig. 3*a*). The steady-state $^{15}N\{^1H\}$-NOEs, and the relaxation times $T_1(^{15}N)$ and $T_2(^{15}N)$ in bPrP(121–230) (Fig. 5) have typical values for a well-structured globular protein of this size. From the T_1/T_2 ratio an overall rotational correlation time of 7.7 ± 1.0 ns was estimated. For the residues 121–127 and 226–230, the decreased $^{15}N\{^1H\}$-NOE values and the longer relaxation times $T_1(^{15}N)$ and $T_2(^{15}N)$ indicate high-frequency rate processes with effective correlation times in the subnanosecond range, and similar results were obtained for the residues 138–144 and 189–199. For these four peptide segments the reduced precision of the structure determination thus correlates with in-

Table 1. Input for the structure calculation and characterization of the energy-minimized NMR structures of the polypeptide segment 121–230 in bPrP(23–230) and bPrP(121–230)

Quantity	Value	
	bPrP(23–230)	bPrP(121–230)
NOE upper distance limits	1,576	1,797
Dihedral angle constraints	469	483
Residual target function, Å²	1.15 ± 0.28	0.79 ± 0.19
Residual NOE violations		
Number ≥0.1 Å	30 ± 5	20 ± 3
Maximum, Å	0.15 ± 0.01	0.14 ± 0.01
Residual angle violations		
Number ≥2.0°	0.4 ± 0.5	0.3 ± 0.4
Maximum, °	2.4 ± 1.1	2.1 ± 0.7
AMBER energies,* kcal/mol		
Total	−4,892 ± 86	−4,952 ± 78
van der Waals	−316 ± 14	−344 ± 9
Electrostatic	−5,208 ± 84	−5,296 ± 76
rms deviation to mean coordinates, Å		
N, C^α, C′ (125–227)	0.78 ± 0.12	0.69 ± 0.11
All heavy atoms (125–227)	1.21 ± 0.11	1.10 ± 0.10

Except for the top two entries the data characterize the group of 20 conformers that is used to represent the NMR structure; the mean value and the standard deviation are given.
*See, for example, ref. 44.

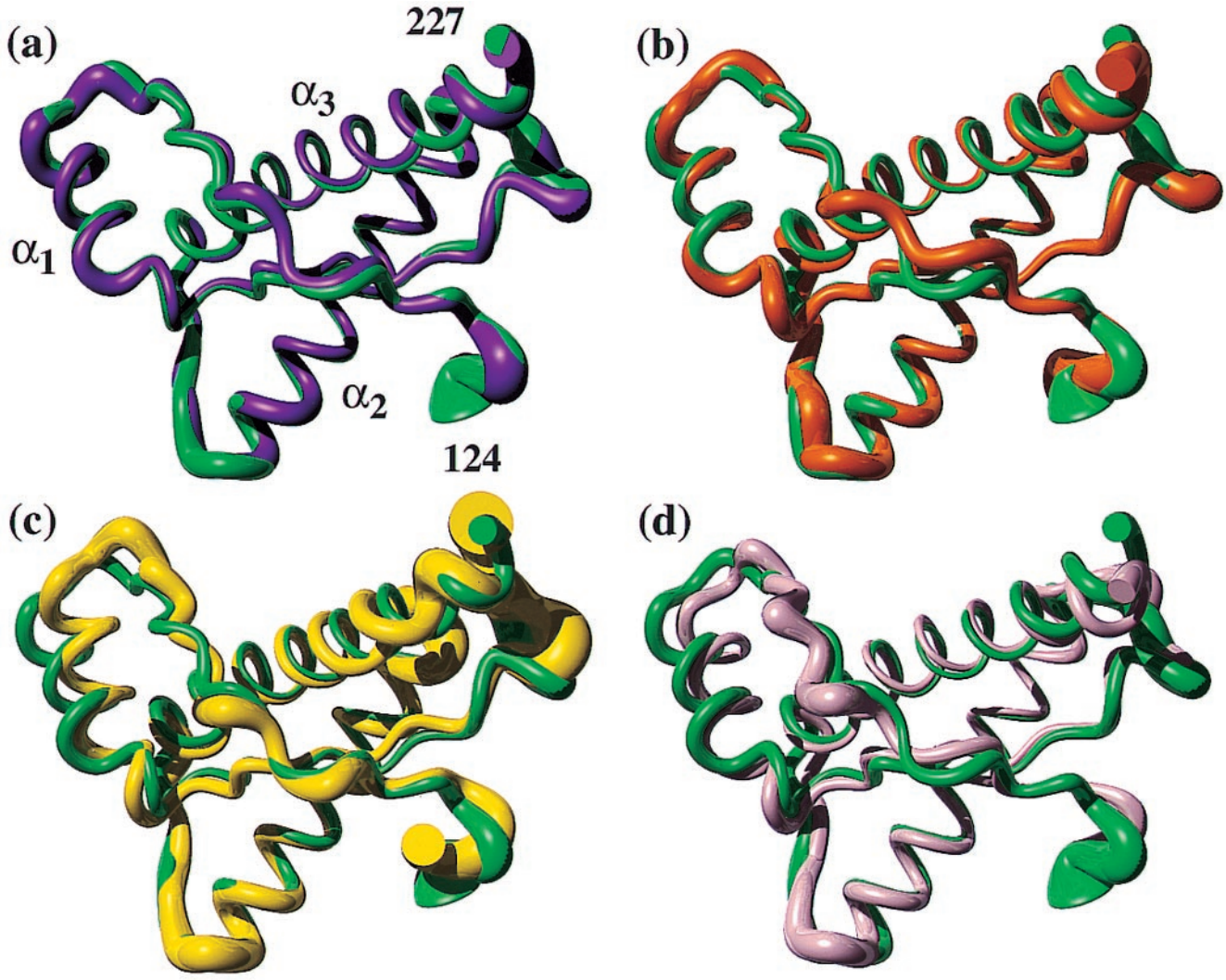

Fig. 3. (*a*) Superposition of the mean NMR structures of the polypeptide segment 124–227 in bPrP(23–230) (violet) and bPrP(121–230) (green). A spline function was drawn through the C^{α} positions. The variable radius of the cylindrical rods is proportional to the mean global backbone displacement per residue (43), as evaluated after superposition for best fit of the atoms N, C^{α}, and C′ of the residues 125–227 in the two bundles of 20 energy-minimized conformers used to represent the solution structures (29). (*b–d*) Superposition of the segment 125–227 in bPrP(121–230) (green) with the corresponding residues in hPrP(121–230) (*b*; orange), mPrP(121–231) (*c*; yellow), and shPrP(90–231) (*d*; pink), respectively.

creased mobility. For the residues 166–173 only an upper limit for the $T_2(^{15}N)$ values could be estimated because of line broadening beyond detection, which seems to arise from slow conformational exchange processes in this segment. The influence of the N-terminal tail on the internal dynamics of the domain is limited to a somewhat reduced mobility of residues 122–124 in bPrP(23–230) (Figs. 2 and 5).

Discussion

The global architecture of bPrP(23–230) (Figs. 1*a* and 2) coincides with the structures of the recombinant human, murine, and Syrian hamster prion proteins (16, 20, 22), implying that conformational transitions between the ubiquitous cellular form and the TSE-related scrapie form follow the same pathway for all four species. With regard to the well-documented species barrier for infectious transmission of prion diseases (14), it is then of interest to investigate possible species-specific local structure variations in this preserved scaffold. Detailed analysis of the available cellular prion protein structures seems highly attractive also in view of possible use of PrP^C as a target for drug development. However, since present knowledge of structure–function correlations in prion proteins consists primarily of the observation that the same polypeptide chain can be found either in PrP^C or PrP^{Sc}, and neither typical protein functions nor possible functional sites have been identified for PrP^C, any search for physiologically relevant structural features should start with a rather broad focus.

Comparison of bPrP, hPrP, mPrP, and shPrP. The structure superpositions in Fig. 3 *b–d* show that the three-dimensional structures of the C-terminal domain in bPrP, hPrP, mPrP, and shPrP are closely similar. hPrP(121–230) is closest to bPrP(121–230), with an rms deviation value of 0.98 Å between the mean structures. The corresponding values for the superpositions of bPrP with mPrP and shPrP are 1.66 Å and 1.68 Å, respectively. Local differences between the backbone conformations are mainly seen near helix 1, and at the end of helix 3 and in the nearby loop of residues 166–172 (Fig. 3 *c* and *d*). The helix 3 in bPrP, hPrP (22), and shPrP (21) is a regular α-helix up to approximately residue 226 (Fig. 3 *a*, *b*, and *d*),

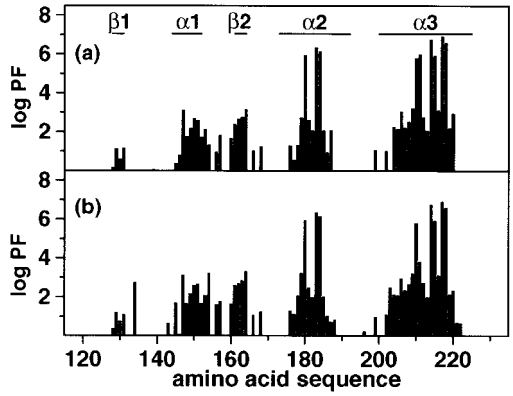

Fig. 4. Logarithmic plots of amide proton exchange protection factors (PF). (*a*) bPrP(23–230). (*b*) bPrP(121–230). Hydrogen–deuterium exchange was measured at 20°C in 99.9% D_2O containing 10 mM sodium acetate at pH 4.5. The locations of the regular secondary structure elements are given in *a*.

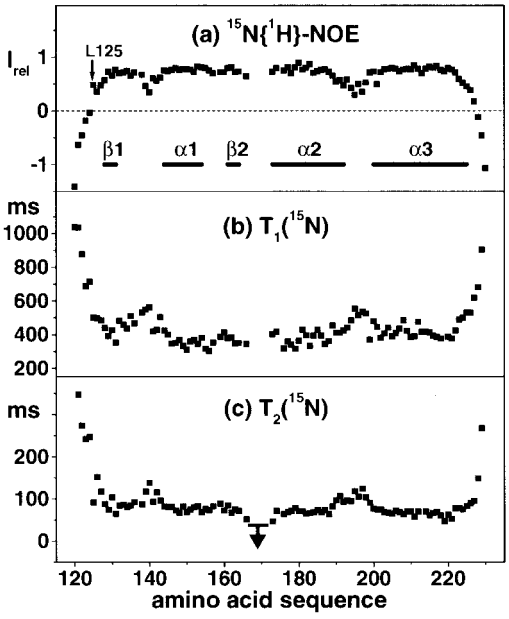

Fig. 5. Data characterizing the internal mobility of the globular domain of bPrP. (*a*) Steady-state $^{15}N\{^1H\}$-NOEs of bPrP(121–230), where Leu-125 is the first residue with a positive NOE. (*b*) Longitudinal ^{15}N spin-relaxation times, $T_1(^{15}N)$. (*c*) Transverse ^{15}N spin-relaxation times, $T_2(^{15}N)$. The arrow indicates an upper limit for $T_2(^{15}N)$ of the residues 166–172. The locations of the regular secondary structure elements are indicated in *a*.

whereas in mPrP (18) there is significant structural disorder from residue 219 onward (Fig. 3*c*). The loop 166–172 is fully NMR-observable only in shPrP (19, 20). These two "conformational markers" (24) are located near the protein surface and actually protrude out of the core of the structure. They therefore show increased structural disorder (Fig. 3) and increased mobility (Fig. 5). Nonetheless, the structure determinations of three variants of hPrP(121–230) described in the following paper (24), which include amino acid exchanges in the loop and in helix 3, showed that the species-specific local conformational variations in this surface area of the protein are significant and can be related to single amino acid exchanges between the different species. On the opposite molecular surface, helix 1 overlaps very closely between bPrP and hPrP (Fig. 3*b*), whereas for mPrP and shPrP it is somewhat displaced toward the core of the protein (Fig. 3 *c* and *d*). Similar to the aforementioned two conformational markers, helix 1 is not as precisely defined as the other two helices (Fig. 3), and it shows lower protection factors for amide proton exchange (Fig. 4).

PrP^C Structure and Species Barriers for Transmission of Prion Diseases. Within the framework of the protein-only hypothesis (11–13), the stringency of the species barrier (34) should be related to the degree of sequence homology between the prion proteins of the host and the infectious material (35, 36). Polypeptide segments that have been proposed to be critical for the susceptibility of PrP^C to transformation into PrP^{Sc} are now known to be located in the globular domain. In particular, the two aforementioned molecular surface regions formed by helix 1, and by the loop 166–172 and helix 3, respectively, have been proposed as sites for intermolecular interactions that might contribute to the species barrier (14, 37, 38). A closer inspection shows that in addition to the near-identity of the backbone of helix 1 between bPrP and hPrP (Fig. 3*b*), the two species have identical sequences in helix 1 and the adjoining loops (refs. 23 and 39; see also the following paper, ref. 24). In contrast, the three sequence positions 143, 145, and 155 in or immediately adjacent to helix 1 show nonconservative amino acid exchanges between bPrP (or hPrP) and either mPrP or shPrP. These variations include Ser/Asn, Tyr/Trp, and His/Tyr or Asn substitutions on the protein surface, which clearly modify the propensity for intermolecular interactions.

In the surface region formed by helix 3 and the loop of residues 166–172, hPrP is unique in carrying a charge of −3, whereas the corresponding charge in the other three species is −1. Similarly, bPrP is unique in carrying a negative charge in position 186, which contains an uncharged, polar residue in the other three species. The resulting different surface charge distributions in bPrP and hPrP are readily apparent in Fig. 1 *c* and *d*, which further illustrates that there are no charge variations between these two species outside of the loop 166–172, position 186 and the C-terminal half of helix 3 (23, 24, 39).

In conclusion, if interactions with the surface area of PrP^C formed by helix 1 are a factor contributing to species barriers, the present comparison of the NMR structures of four prion proteins indicates that this contribution to the barrier between cattle and humans would be very small or completely absent, whereas its impact could be rather important for the barrier between either of these two species and the mouse or the Syrian hamster. Similar considerations for the PrP^C surface areas formed by the loop 166–172, residue 186, and the C-terminal part of helix 3 indicate that contributions to a species barrier between humans and cattle would have to be due to different surface charge distributions, whereas conformational differences might contribute to or even represent a dominant factor in the species barriers between cattle (or humans) and mice or Syrian hamsters (2, 37, 38), as well as between mice and Syrian hamsters (35, 36, 40, 41). It remains to be seen in what ways the identification of surface charge variation as the sole relevant feature of the PrP^C structure with regard to the species barrier between humans and cattle could be exploited for gaining further insight into the role of PrP^C in the determination of species barriers, and perhaps for outlining novel avenues for assessing or even modifying the barrier for transmission of prion diseases between specified species combinations.

We thank Christine von Schroetter for technical help with the protein preparation, Martin Billeter and Peter Güntert for advice with the structure calculations, and Martha Geier for the careful processing of the manuscript. Financial support was obtained from the Schweizerischer Nationalfonds (Projects 31.49047.96 and 438+050287).

1. Will, R. G., Ironside, J. W., Zeidler, M., Cousens, S. N., Estibeiro, K., Alperovitch, A., Poser, S., Pocchiari, M., Hofman, A. & Smith, P. G. (1996) *Lancet* **347,** 921–925.
2. Collinge, J., Palmer, M. S., Sidle, K. C. L., Hill, A. F., Gowland, I., Meads, J., Asante, E., Bradley, R., Lawrence, J. D. & Lantos, P. (1995) *Nature (London)* **378,** 779–783.
3. Collinge, J., Sidle, K. C. L., Meads, J., Ironside, J. & Hill, A. F. (1996) *Nature (London)* **383,** 685–690.
4. Bruce, M. E., Will, R. G., Ironside, J. W., McConnell, I., Drummond, D., Suttie, A., McCardle, L., Chree, A., Hope, J., Birkett, C., *et al*. (1997) *Nature (London)* **389,** 498–501.
5. Hill, A. F., Desbruslais, M., Joiner, S., Sidle, K. C. L., Gowland, I., Collinge, J., Doey, L. J. & Lantos, P. (1997) *Nature (London)* **389,** 448–450.
6. Collinge, J. (1999) *Lancet* **383,** 685–690.
7. Scott, M. R., Will, R., Ironside, J., Nguyen, H. O. B., Tremblay, P., DeArmond, S. J. & Prusiner, S. B. (1999) *Proc. Natl. Acad. Sci. USA* **96,** 15137–15142.
8. Will, R. G., Cousens, S. N., Farrington, C. P., Smith, P. G., Knight, R. S. G. & Ironside, J. W. (1999) *Lancet* **353,** 979.
9. Ridley, R. M., Baker, H. F. & Windle, C. P. (1996) *Lancet* **348,** 56.
10. Bons, N., Mestre-Frances, N., Belli, P., Cathala, F., Gajdusek, D. C. & Brown, P. (1999) *Proc. Natl. Acad. Sci. USA* **96,** 4046–4051.
11. Alper, T., Cramp, W. A., Haig, D. A. & Clarke, M. C. (1967) *Nature (London)* **214,** 764–766.
12. Griffith, J. S. (1967) *Nature (London)* **215,** 1043–1044.
13. Prusiner, S. B. (1982) *Science* **216,** 136–144.
14. Prusiner, S. B. (1998) *Proc. Natl. Acad. Sci. USA* **95,** 13363–13383.
15. Riek, R., Hornemann, S., Wider, G., Billeter, M., Glockshuber, R. & Wüthrich, K. (1996) *Nature (London)* **382,** 180–182.
16. Riek, R., Hornemann, S., Wider, G., Glockshuber, R. & Wüthrich, K. (1997) *FEBS Lett.* **413,** 282–288.
17. Billeter, M., Riek, R., Wider, G., Hornemann, S., Glockshuber, R. & Wüthrich, K. (1997) *Proc. Natl. Acad. Sci. USA* **94,** 7281–7285.
18. Riek, R., Wider, G., Billeter, M., Hornemann, S., Glockshuber, R. & Wüthrich, K. (1998) *Proc. Natl. Acad. Sci. USA* **95,** 11667–11672.
19. James, T. L., Liu, H., Ulyanov, N. B., Farr-Jones, S., Zhang, H., Donne, D. G., Kaneko, K., Groth, D., Mehlhorn, I., Prusiner, S. B. & Cohen, F. E. (1997) *Proc. Natl. Acad. Sci. USA* **94,** 10086–10091.
20. Donne, D. G., Viles, J. H., Groth, D., Mehlhorn, I., James, T. L., Cohen, F. E., Prusiner, S. B., Wright, P. E. & Dyson, H. J. (1997) *Proc. Natl. Acad. Sci. USA* **94,** 13452–13457.
21. Liu, H., Farr-Jones, S., Ulyanov, N. B., Llinas, M., Marquesee, S., Groth, D., Cohen, F. E., Prusiner, S. B. & James, T. L. (1999) *Biochemistry* **38,** 5362–5377.
22. Zahn, R., Liu, A., Lührs, T., Riek, R., von Schroetter, C., López García, F., Billeter, M., Calzolai, L., Wider, G. & Wüthrich, K. (2000) *Proc. Natl. Acad. Sci. USA* **97,** 145–150.
23. Schätzl, H. M., Da Costa, M., Taylor, L., Cohen, F. E. & Prusiner, S. B. (1995) *J. Mol. Biol.* **245,** 362–374.
24. Calzolai, L., Lysek, D. A., Güntert, P., von Schroetter, C., Riek, R., Zahn, R. & Wüthrich, K. (2000) *Proc. Natl. Acad. Sci. USA* **97,** 8340–8345.
25. Zahn, R., von Schroetter, C. & Wüthrich, K. (1997) *FEBS Lett.* **417,** 400–404.
26. Bai, Y., Milne, J. S., Mayne, L. & Englander, S. W. (1993) *Proteins* **17,** 75–86.
27. Farrow, N. A., Muhandiram, R., Singer, A. U., Pascal, S. M., Kay, C. M., Gish, G., Shoelson, S. E., Pawson, T., Forman-Kay, J. D. & Kay, L. E. (1994) *Biochemistry* **33,** 5984–6003.
28. Orekhov, V. Y., Nolde, D. E., Golovanov, A. P., Korzhnev, D. M. & Arseniev, A. S. (1995) *Appl. Magn. Reson.* **9,** 581–588.
29. Wüthrich, K. (1986) *NMR of Proteins and Nucleic Acids* (Wiley, New York).
30. Bax, A. & Grzesiek, S. (1993) *Acc. Chem. Res.* **26,** 131–138.
31. Senn, H., Werner, B., Messerle, B. A., Weber, C., Traber, R. & Wüthrich, K. (1989) *FEBS Lett.* **249,** 113–118.
32. Neri, D., Szyperski, T., Otting, G., Senn, H. & Wüthrich, K. (1989) *Biochemistry* **28,** 7510–7516.
33. Güntert, P., Mumenthaler, C. & Wüthrich, K. (1997) *J. Mol. Biol.* **273,** 283–298.
34. Pattison, I. H. (1965) in *Slow, Latent and Temperate Virus Infections,* eds. Gajdusek, D. C., Gibbs, C. J., Jr., & Alpers, M. P. (U.S. Government Printing Office, Washington, DC), NINDB Monograph 2, pp. 249–257.
35. Scott, M., Foster, D., Mirenda, C., Serban, D., Coufal, F., Wälchi, M., Torchia, M., Groth, D., Carlson, G., DeArmond, S. J. & Westaway, D. (1989) *Cell* **59,** 847–857.
36. Scott, M., Groth, D., Foster, D., Torchia, M., Yang, S. L., DeArmond, S. J. & Prusiner, S. B. (1993) *Cell* **73,** 979–988.
37. Telling, G. C., Scott, M., Hsiao, K. K., Foster, D., Yang, S., Torchia, M.-L., Sidle, K. C. L., Collinge, J., DeArmond, S. J. & Prusiner, S. B. (1994) *Proc. Natl. Acad. Sci. USA* **91,** 9936–9940.
38. Telling, G. C., Scott, M., Mastrianni, J., Gabizon, R., Torchia, M., Cohen, F. E., DeArmond, S. J. & Prusiner, S. B. (1995) *Cell* **83,** 79–90.
39. Wopfner, F., Weidenhöfer, G., Schneider, R., von Brunn, A., Gilch, S., Schwarz, T. F., Werner, T. & Schätzl, H. M. (1999) *J. Mol. Biol.* **289,** 1163–1178.
40. Kaneko, K., Zulianello, L., Scott, M., Cooper, C. M., Wallace, A. C., James, T. L., Cohen, F. E. & Prusiner, S. B. (1997) *Proc. Natl. Acad. Sci. USA* **94,** 10069–10074.
41. Kimberlin, R. H., Walker, C. A. & Fraser, H. (1989) *J. Gen. Virol.* **70,** 2017–2025.
42. Koradi, R., Billeter, M. & Wüthrich, K. (1996) *J. Mol. Graphics* **6,** 1–10.
43. Billeter, M., Kline, A. D., Braun, W., Huber, R. & Wüthrich, K. (1989) *J. Mol. Biol.* **206,** 677–687.
44. Case, D. A., Pearlman, D. A., Caldwell, J. W., Cheatham, T. E., III, Ross, W. S., Simmerling, C. L., Darden, T. A., Merz, K. M., Stanton, R. V., Cheng, A. L., *et al.* (1997) AMBER 5.0 (University of California, San Francisco).